Proceedings of the Combustion Institute 42 (2026) 106369

Contents lists available at ScienceDirect

Proceedings of the Combustion Institute

journal homepage: www.elsevier.com/locate/proci

Investigation of liquid fuel film cooling under rocket-like conditions using laser-induced fluorescence

Matthias Koegl *, Bjarne Andersson, Christopher Horsch, Markus Gerhard Klatt, Lars Zigan

Institut für Thermodynamik, Professur für Energiewandlung, Fakultät für Luft- und Raumfahrttechnik, Universität der Bundeswehr München (UniBw M), D-85577 Neubiberg, Germany

ARTICLE INFO

Keywords:
Liquid film cooling
Temperature
Fluorescence

ABSTRACT

The present paper investigates a liquid film cooling process under rocket-like conditions in a pulsejet engine. The fuel-based coolant mixture (90 vol.% isooctane, 10 vol.% ethanol, doped with the fluorescence tracer Nil red) is injected under 30° through a 1 mm orifice onto the wall to shield it from hot exhaust gas flow (~1070 K, ~ 95 m/s). The highly transient film cooling process is analyzed in two perspectives: a lateral view with 1-color laser-induced fluorescence (LIF) imaging provides film structural and thickness information. A top view of the film provides details of film temperature distribution using a two-color LIF detection scheme. The 2-color LIF technique is calibrated in a separate flow cell. The investigated operating points show a highly fluctuating outlet behavior of the fuel stream due to the turbulent gas flow, which has a significant impact on the liquid film formation downstream. A higher liquid flow rate leads to a more compact, less disrupted fuel stream at the orifice exit with a larger effective cooling film length. Strong interaction with the impinging hot exhaust gas cross flow leads to formation of large ligaments at the orifice exit and frequent occurrence of ignition and combustion events in the jet. Additionally, the larger reaction surface leads to locally occurring diffusive combustion of the film further downstream for all operating points. The maximal determined liquid temperature within the investigated field of view is in the range of the boiling temperature of isooctane (373 K) for operating points with large liquid flow rate. However, superheated liquid was observed for the operating point with low liquid mass flow. These conditions lead to spherical widening of the liquid jet in the near nozzle regions, which could be due to micro-explosions (or "puffing").

Novelty and significance statement: So far, no planar LIF measurements on liquid cooling film temperature and structure were conducted at high gas temperatures (≥ 1000 K) inside a combustor. The present paper provides detailed insights into the heat transfer mechanisms in liquid film cooling configurations at high temperature and gas velocity. For this purpose, an optically accessible combustion test rig was designed providing a high temperature, high velocity reactive gas atmosphere. Planar 2-color LIF was calibrated and applied in the combustor for liquid film temperature and structure measurements at very challenging combustion conditions with local ignition and "puffing" (i.e. micro-explosions) or burst of the liquid film. The details of film formation, its thickness, temperature and breakup allow for better understanding of the film stability and its modeling.

1. Introduction

In combustion chambers of thrusters, the reaction of fuel and oxidizer leads to very high gas and wall temperatures, which may exceed 3000 K. Consequently, different techniques exist to protect the wall of the combustion chamber such as regenerative cooling, film or transpiration cooling, ablation, endothermic heat sinks etc. [1]. Film cooling is a feasible measure to protect the walls [2], which is especially relevant for small rocket engines in which regenerative cooling of the combustor wall is not reasonable [3]. In case of liquid rocket engines, a thin liquid coolant film is formed by jet or spray impingement under a certain angle to the wall or by fuel introduction through small openings in the wall [4, 5]. The produced liquid film on the combustor chamber wall should cover a large area for efficient wall cooling. The convective heat transfer from the hot exhaust gas leads to increased liquid film temperature and evaporation rate as well as reduced film thickness further downstream. Furthermore, the film temperature and thickness are affected by the latent heat of the liquid and the high gas velocity of the hot gas flow. The

* Corresponding author.
E-mail address: matthias.koegl@unibw.de (M. Koegl).

https://doi.org/10.1016/j.proci.2026.106369
Received 9 March 2026; Accepted 8 June 2026
Available online 15 September 2026
1540-7489/© 2026 The Author(s). Published by Elsevier Inc. on behalf of The Combustion Institute. This is an open access article under the CC BY license (http://creativecommons.org/licenses/by/4.0/).

covered area of the film and the corresponding cooling effectiveness is controlled by the momentum ratio (or blowing ratio) of the gas flow and the liquid film. The fuel mass flow must be large enough to improve the cooling but minimal enough to improve the specific impulse. Large shear flow between liquid and gas leads to wavy films and changed heat transfer characteristics. Especially, strong evaporation of very thin liquid films may lead to rivulet flows and local dry out, which potentially can result in damages of the combustor wall.

For optimization of the film cooling, a physical understanding of the film formation and evaporation is required. Consequently, optical accessible test rigs and preferably laser-based imaging techniques are necessary to investigate the local heat transfer and the film quantities. These include the film area and structure as well as liquid temperature and thickness. Up to now, many film dynamics measurements were conducted under simplified conditions, which are not comparable to the realistic behavior in the combustor. Very often, water or ethanol (with "similar" fluid properties as the rocket propellant Monomethylhydrazine (MMH)) films are experimentally studied at relatively low gas and wall temperatures, i.e. below the boiling temperature of the liquid. Mainly integral optical techniques are applied, which do not provide spatially resolved information of film temperature, thickness and structure. For example, backlight illumination was applied [6] for studying Kelvin–Helmholtz and Rayleigh–Taylor instabilities in the water film for electrically heated gas flows at up to 440 K. Hu et al. [7] used the same technique for studying water film shapes as well as temperature profiles using thermocouples in an impinging jet configuration. Infrared thermography was applied by Liu et al. [8] to study wall temperatures at the rear surface when covered with liquid films. Initial wall temperatures were 313 K to 393 K and ambient air temperature was 293 K. Fuji et al. [2] applied backlight illumination to study MMH film front velocity, film thickness and length inside an optically-accessible combustion chamber operated at fired conditions.

Brightness-based laser-induced fluorescence (LIF) was applied by Liu et al. [9] to study the water film formation and thickness under isothermal cold conditions. Soller et al. [3] point-wise measured the local film temperature using a two-color-two dye LIF technique. Ethanol fuel films were studied in an electrically heated air flow at 500 K and 600 K at blowing ratios M ranging from 3.2 to 17.7. The conditions were chosen in order to avoid ignition and combustion of the cooling film.

So far, no planar LIF measurements on liquid film temperature and structure were conducted at much larger gas temperatures inside a combustor. This is part of the present paper in order to get detailed insights into the heat transfer mechanisms in liquid film cooling configurations. For this purpose, an optically accessible combustion test rig was designed providing a high temperature, high velocity reactive gas atmosphere. A planar 2-color LIF technique was calibrated and applied in the combustor for liquid film temperature and structure measurements at very challenging combustion conditions with local ignition and "puffing" or burst of the liquid film.

2. Experimental setup

The experimental setup for the investigation of the fuel wall film is shown in Fig. 1. The hot exhaust flow generated by a pulsejet engine (exhaust inner diameter: 43 mm), is guided smoothly with a conical transition of 100 mm length through the quadradic cross section of the optically accessible measurement section (42 mm x 42 mm, edge radius 6.5 mm).

The setup generates gas temperatures of up to about 1070 K and exhaust gas velocities up to about 100 m/s in the measurement section. The pulse frequency is 170 Hz with a pressure amplitude of 14 kPa (pressure sensor model: 13B28, PCB, Germany). The operating conditions are monitored by pressure sensors and thermocouples. A pulsed Nd:YAG laser (model: Q-smart 850, Quantel, France, wavelength: 532 nm, laser fluence 1.32 mJ/cm^2) is used to volumetrically excite the dye Nile red in the liquid in the probe region. The laser fluence was

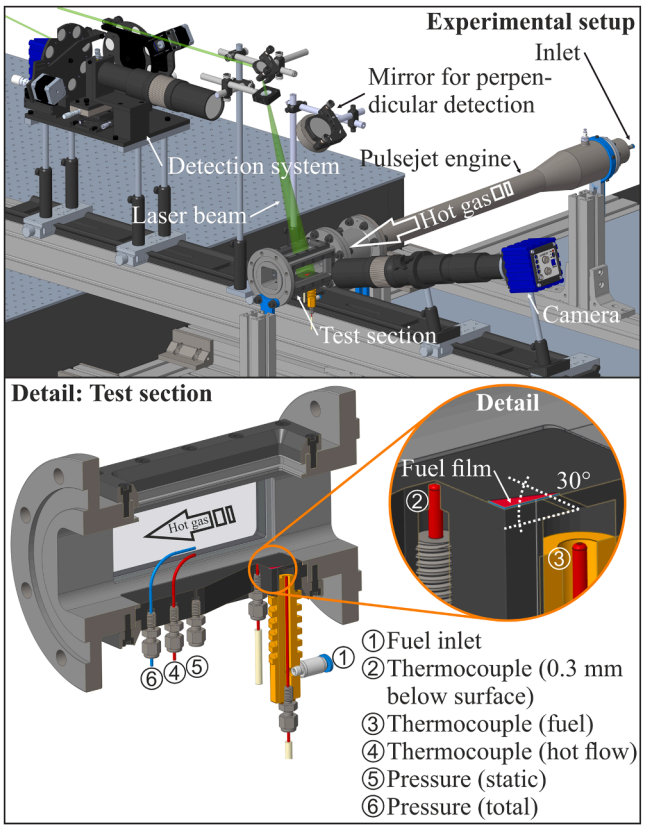


Fig. 1. Experimental setup (top) with detail view of optically accessible test section (bottom).

simultaneously monitored by a power meter (model: UP55N-40S-H9-INT-D0, Gentec Electro-Optics, Canada). The probe region is illuminated under a 75° angle to enable a perpendicular signal acquisition with the 2c-LIF detection system. To evaluate the dye concentration and the respective bandpass filters, a precedent study was conducted. Here, the temperature dependent fluorescence signal is investigated with a spectroscopic setup, which is described in Ref. [10].

The film measurements are conducted with three identical sCMOS cameras (model: Imager, LaVision GmbH, Germany). Two cameras for 2c-PLIF are combined in a detection system, which is equipped with a long-range microscope (model: Distamax K2, Infinity, USA, nominal pixel resolution: 96.7 pixel/mm, field of view (FoV): 26.5 mm x 22.3 mm) to capture the volumetric fluorescence signal perpendicularly to the film surface. Two well selected bandpass filters (575 nm and 650 nm, 50 nm FWHM, OD4, Edmund Optics, NY, USA) directly in front of the cameras enable a determination of the film temperature after calibration (see below). A third individual camera, which is also equipped with a long-range microscope (model: Distamax K2, Infinity, USA, nominal pixel resolution: 294.3 pixel/mm, FoV: 8.69 mm x 7.34 mm) and a 532 nm notch filter (533 nm, 17 FWHM, Thorlabs, USA) monitors the film structure closer at the orifice outlet from the side at an angle of 20° The combustion pictures are taken under the same detection angle with a DSLR camera (camera model: EOS 5D Mark IV, Canon, Japan; objective model: EF 24–105 mm 1:4 L IS II USM, Canon, Japan, nominal pixel resolution: 13.37 pixel/mm).

2.1. Test section

The test section (see Fig. 1 bottom) features three sapphire windows (optical access: 98 mm x 33 mm) and one flange (stainless steel, material no 1.4301, glass bead blasted surface), where the film generation takes place. The fluorescence light reflection behavior of this wall material

was already investigated in [10]. The velocity of the exhaust gas in the center of the measurement section is determined with two pressure sensors (model: S20, 0.16 MPa abs, WIKA, Germany). The fuel for the film generation is pumped with a syringe pump (model: NE1010, New Era Pump Systems, Inc., USA) and exits the plate under a 30° angle (bore diameter: 1 mm, elliptical exit: 2 mm x 1 mm). The temperature of the injected fuel, the wall (thermocouple positioned 0.3 mm below surface) and the hot gas are measured with thermocouples (type K; diameter 1.5 mm, TC-direct, Germany).

The pulsejet engine is driven by pure isooctane, which is a suitable substitute fuel for MMH and kerosene, while the 2c-PLIF film study is conducted with a mixture of 90 vol.% isooctane and 10 vol.% ethanol to ensure a sufficient solubility of the dye Nile red in the fuel. Here a concentration of 25 mg/L (78.6 µmol/L) ensures a linear fluorescence signal depending on the amount of dye dissolved in the liquid. The authors already investigated the solubility, absorption and fluorescence of Nile red in kerosene (Jet-A1) in an earlier study and compared it to model fuels including isooctane [11]. After adequate calibration, the technique could also be applied for Jet-A1.

Nile red has a melting point of 476 K −479 K [12], which is below the determined film temperatures in the present paper.

3. Results

This section is structured as follows: First the LIF signal depending on the temperature was calibrated spectrally and by imaging in a flow cell (details of the setup can be found in Ref. [10]. Afterwards, the cooling film formation process is investigated and the film temperature distribution is determined using LIF. Finally, chemiluminescence imaging in the visible spectral range provides information about premixed and non-premixed combustion in the cooling jet and film regions.

3.1. Temperature dependent calibration

The temperature of the liquid-dye mixture can be determined with the intensity ratio r of the two channels of the detection system CH1 and CH2, respectively. We determined the intensity ratios for 25 mg/L Nile red in E10 in a calibration flow cell using the same spectroscopic setup as in reference [10]. The intensity ratio r can be determined using the ratio of the two products of the transmission curves τ of the respective filters and the spectral fluorescence emissions I_{Ch1} and I_{CH2}: (when other efficiencies of the optical setup (e.g., cameras) are neglected):

$$r = \frac{\sum \tau_{Filter_575nm} \cdot I_{LIF}}{\sum \tau_{Filter_650nm} \cdot I_{LIF}} = \frac{I_{CH1}}{I_{CH2}} \quad (1)$$

The normalized spectral LIF emission signals of 25 mg/L Nile red in the fuel mixture at 0.5 mm film thickness using a special calibration flow cell (experimental setup see [10]) are shown in Fig. 2 together with the selected bandpass filters that are applied for the temperature determination.

The emission signals are characterized by broad-band spectra with single peaks. A temperature increase shifts the fluorescence peak (293 K: 621.7 nm and 343 K: 602.8 nm) and both flanks equally towards shorter wavelengths. The selected bandpass filters enable a quantitative temperature determination via the intensity ratio within the fuel film after calibration using the camera system.

The broader emission bands in comparison to theoretically available narrower band pass filters reduce the thermal sensitivity, but are indispensable for achieving a sufficient large signal-to-noise ratio under pulsed illumination and short camera integration times especially for thin liquid films [13].

3.2. LIF imaging measurements

The camera-based detection system has a different efficiency (filters, lenses, mirrors and quantum efficiency of the sCMOS, etc.) in comparison to the spectroscopic setup. Consequently, the temperature dependent calibration has to be repeated to ensure highest measurement accuracy and precision. The average intensities of a square area in the center of the measurement volume (351 pixels x 351 pixels) were used for the evaluations. The calibration function and the corresponding temperature sensitivity of the 2c-PLIF technique are presented in Fig. 3.

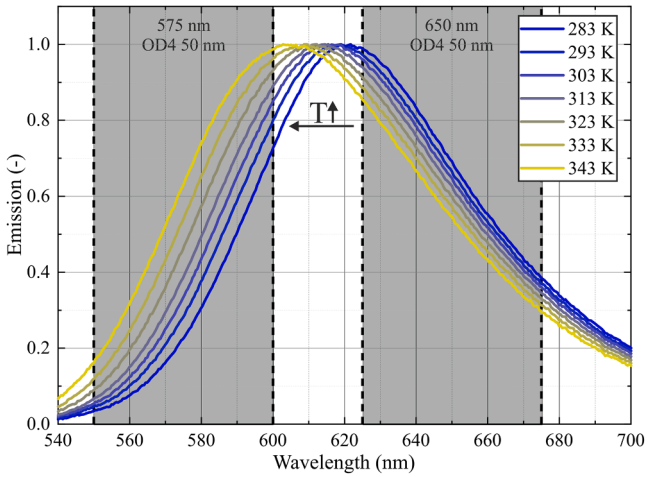


Fig. 2. Normalized emission spectra of 25 mg/L Nile red dissolved in the isooctane ethanol mixture at 0.5 mm film thickness in the flow cell for various temperatures; chosen BP filters for calculation of the intensity ratio marked in grey.

The temperature T_{Film} can be determined by the intensity ratio r with the following polynomial equation (coefficient of determination: R^2=0.99993):

$$T_{Film} = 187.77 + 371.69 \cdot r - 342.40 \cdot r^2 + 129.28 \cdot r^3 \quad (2)$$

The signal ratio monotonously rises with temperature and the sensitivity is always above 1.45 %/K in the studied temperature range, which is similar or larger than other 2c-LIF techniques based on dyes such as Rhodamine B in ethanol (concentration: 2.5µmol/L, 0.7 %/K, [14]) and pyrromethene PM597 in ethanol (concentration: 10 µmol/L, 1.2 %/K, [15]).

3.3. Film measurements in the combustor

The cooling film formation in terms of liquid dispersion at the orifice exit and film temperature distribution is analyzed in the following

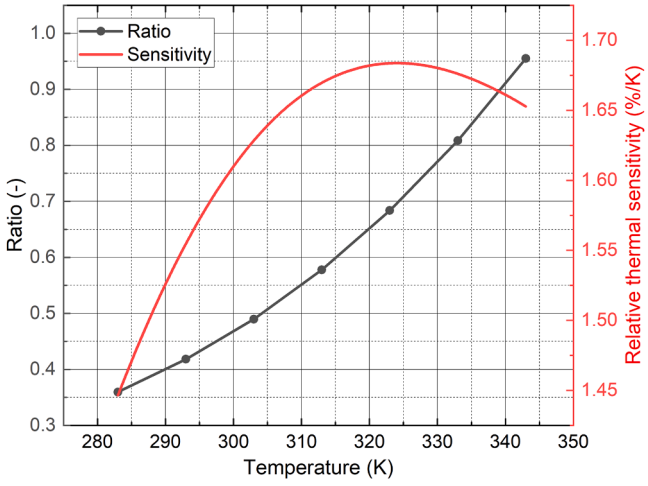


Fig. 3. Temperature-sensitive PLIF intensity ratio and corresponding relative temperature sensitivity.

section based on three different operating points (OPs). The injection conditions and the corresponding characteristic non-dimensional parameters in terms of Reynolds and Weber number, blowing and momentum ratio of the different operating points are shown in Table 1. The Reynolds and Weber number are calculated with the properties of pure isooctane. The blowing and momentum ratio with the density of E10 at 290 K.

The hot gas velocity and gas temperature are measured just before the fuel injection is started. The fuel temperature is measured in the plenum before the channel. The locations of all temperature and pressure measurements are shown in Fig. 1. The Reynolds number $Re = (D_e .U_e)/\nu_F$, the Weber number $We = (\rho_e .U_e^2 D_e)/\sigma_e$, the blowing ratio $M = (\varrho_e .U_e)/(\varrho_\infty .U_\infty)$ and the momentum flux ratio $J = (\varrho_e .U_e^2)/(\varrho_\infty .U_\infty^2)$, where the subscript "$e$" represents the jet exit conditions and "∞" the free stream conditions, are calculated as well. The slightly varying hot gas velocities are attributed to the pulsejet engine operation, which is very sensible regarding slightly changing ambient conditions in the lab. The larger liquid mass flow and consequently larger Reynolds and Weber number could be advantageous in forming a larger cooling film at the wall. However, the jet may also lift off anddisintegrate into smaller liquid structures at larger liquid flow rate.

The liquid jet and film structure in the orifice region (zoomed side view), the LIF signals and the corresponding signal-to-noise ratios ($SNR=I_{Signal}/I_{Noise}$) of the two detection channels CH1 (575 nm) and CH2 (650 nm) and the determined temperature distribution in the measurement volume (top view) are shown for two individual single-shot events for the three operating points studied in Fig. 4.

The single-shot LIF signals at the orifice outlet reveal that the liquid jet and film structure of the exiting fuel stream strongly fluctuates with time due to the interaction with the turbulent, high-speed gas crossflow. A larger liquid flow rate leads to a denser fuel stream with higher momentum (J, see *Table 1*), which effectively reduces the turbulent breakup (which are mainly induced by Kelvin-Helmholtz instabilities) of the liquid stream and consequently lowers the reaction surface with the hot gas. A decrease in liquid volume flow leads to a more disrupted fuel stream with ligaments and larger wrinkling of the surface due to interaction of the pulsating, turbulent hot gas cross flow. The cooling film evaporation and mixing with hot ambient gas is faster, which is followed by ignition and combustion.

An analysis of the two detection channels CH1 and CH2 reveals that the film length increases with increasing volume flow. In general, the radial film boundaries are better visible in CH1. In the case of OP1 the film signal fades within the investigated field of view (top view), while OP2 and OP3 show a LIF signal in the whole field of view. The overall lower signal intensities of CH1 lead to lower spatial SNRs in comparison to CH2. The large signal intensities at the nozzle outlet and at locations slightly downstream, where still large film thicknesses are present (mainly for OP3), show relatively high SNRs (up to about 10). The thin film regions at the borders and further downstream are characterized by similar lower SNRs (~ 3) for all investigated OPs. The signal intensities of CH1 and CH2 at the edge regions and further downstream are very low (see Fig. 4), which indicates a small liquid film thickness in these specific regions. Therefore, the low SNRs may lead to locally higher measurement errors of the film temperature in these regions. The temperature determination is derived out of the two background corrected detection channels (background ~ 300 counts) with a threshold of 200 counts prior the ratio formation, to reduce high measurement errors in the temperature field in low SNR regions (see Fig. 4). An analysis of the temperature distribution (bottom line) shows that the hot gas and wall preheat the liquid (initially at 290 K) in the fuel duct at the orifice for lower volume flows (OP1: 340 K, OP2: 310 K). The high-volume flow at OP3 (294 K) shows only a slight temperature increase in the fuel duct. The mixture with hot ambient gas increases the temperature of the fuel film with distance to the orifice downstream and towards the edge regions. Generally, a reduction in fuel volume flow leads to a reduction of the formed fuel film length and its film velocity and therefore to a temperature increase of the fuel itself and the wall temperature (wall temperature at thermocouple 2 (see Fig. 1) OP1: 395 K → OP3: 363 K). The liquid temperature distributions revealed that a sufficient cooling effect of the wall can only be achieved for OP2 and OP3, since the volume flow of OP1 is too low for formation of a sufficiently large film. The temperature distributions in the film are analyzed in detail in the time averaged temperature distributions (see Fig. 5, Fig. 6). The maximal expected liquid temperature is in the range of the boiling temperature of isooctane (373 K). However, the temperature distributions show temperatures above 373 K at the edge regions and further downstream, especially for OP1. It should be noted that the fuel is auto-ignited downstream leading to droplet combustion, while a premixed flame is formed at the outlet of the test section (see Fig. 7). Measurements without laser illumination revealed, that the flame luminosity is not detected by the two detection channels due to the short integration times of the sCMOS cameras and sufficient bandpass filters.

The temperature distribution of the film and possible non-premixed film or droplet combustion within the field of view are strongly dependent on the structure of the exiting fuel jet and its attachment to the wall. The lower flow rates of OP1 and OP2 lead to larger interaction surfaces to the hot gas and reduces the distance downstream, from where partial diffusive combustion of the film takes place. Additionally, the top view temperature distribution shows frequently a local spherical widening of the films further downstream (see Fig. 4, 1.1, 1.2, 2.2 bottom line), which appear like "eruptions". These structures are probably not generated by the turbulent flow alone, but could be due to "puffing" of the liquid structures, which was also reported in harsh combustion environments of diesel sprays and in spray flame synthesis [18,19]. This phenomenon will be addressed further in the subsequent paragraphs.

Fig. 5 presents the average LIF signal of the liquid dispersion in the orifice region (top row) and the average temperature distribution (third row) with the corresponding coefficients of variation (COV, second and fourth row, respectively) of 100 consecutively images for the investigated operating points. The corresponding temperature plots along the center lines are shown in Fig. 6.

The average LIF signals of the liquid phase in the orifice region show a lift of the fuel stream trajectory with increasing volume flow, see Fig. 5.

The COV shows lower values in the stream center (trajectory) and higher values at the outer regions, where the hot gas cross flow impinges the surface of the exiting fuel stream. The COV values at the stream core decrease with increasing volume flow due to a denser and less fluctuating disrupted fuel stream core (see also single-shot images in Fig. 4). The bulk areas of the fuel jet and film show a lower temperature in comparison to the edge areas, which was already reported for the single-shot images (see Fig. 4). The COV of the fuel film temperature distribution reveals that the temperature fluctuation increases from the center

Table 1
Operating conditions [16,17].

Property	Unit	OP1	OP2	OP3
Hot gas velocity	m/s	94	98	92.3
Hot gas temperature	K	1085	1070	1000
Surface temperature (location ② in Fig. 1)	K	395	373	363
Fuel temperature in plenum	K	290	290	290
Fuel temperature at outlet	K	350	314	297
Fuel surface tension at outlet σ_e	kg/s	0.0138	0.0170	0.0186
Kinematic viscosity of fuel ν_F	mm^2/s	0.448	0.599	0.698
Fuel density at outlet ρ_e	kg/m^3	644.75	674.52	688.74
Mass flow of fuel (cooling film)	mL/min	30	60	120
Exit velocity *Ue*	m/s	0.636	1.27	2.54
Reynolds number *Re*	-	1418.9	2120.4	3637.0
Weber number *We*	-	18.9	64.0	238.9
Blowing ratio *M*	-	15.2	29	61.8
Momentum flux ratio *J*	-	0.10	0.38	1.69

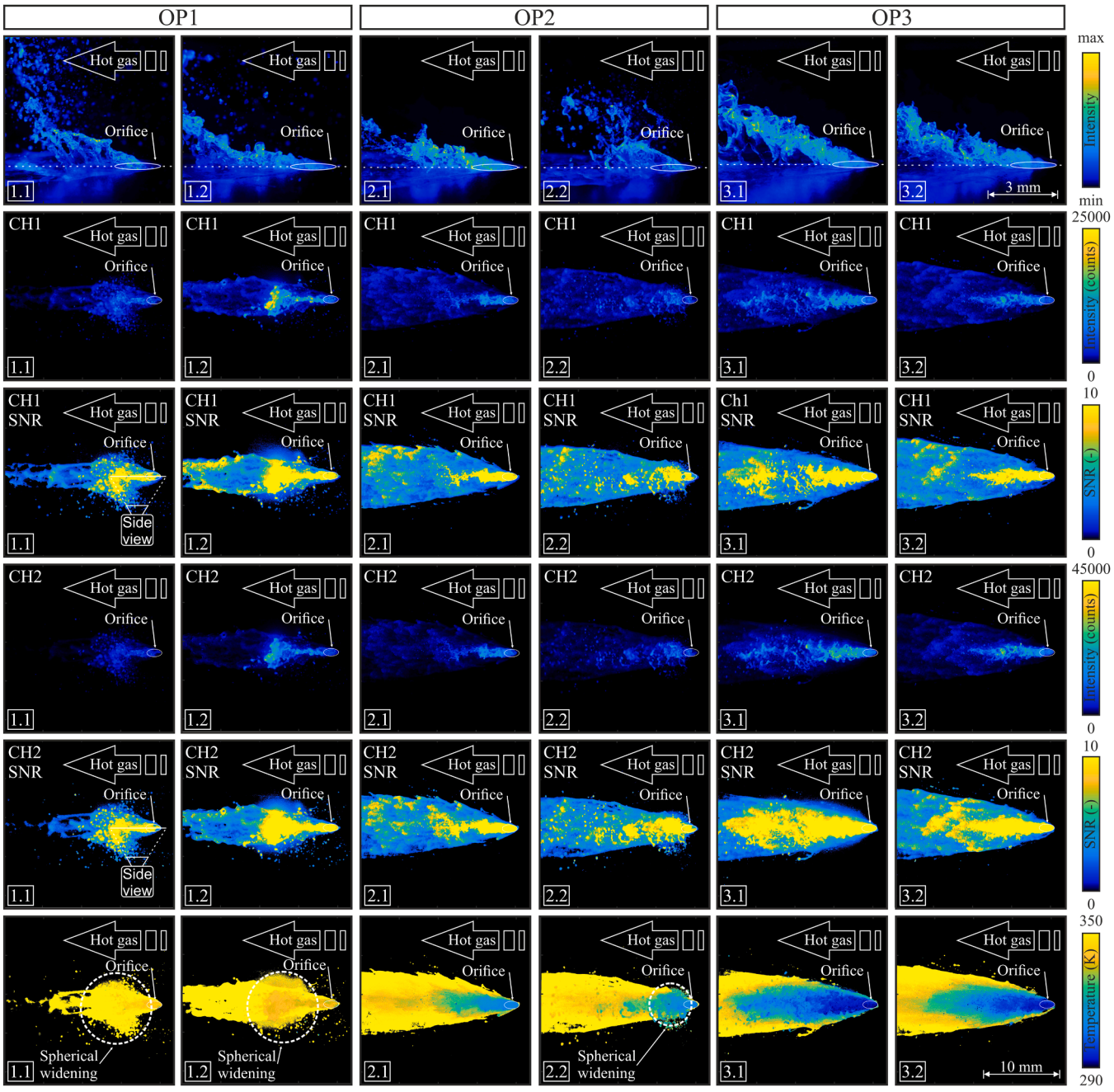


Fig. 4. Zoomed orifice region (side view, first row) and corresponding signal intensities with SNR and temperature distribution in the liquid (top view, second to fourth row) for two single-shot events for each operating point.

line towards the film borders and with increasing distance from the orifice outlet. This is caused by the increasing influence of the hot exhaust gas crossflow on the film formation and aerodynamic breakup.

The temperature plot along the center axis (width: 1 pixel, see Fig. 6) enables an evaluation of the effective cooling length of the fuel films. The effective cooling length describes the film length, where the determined film temperature is below the evaporation temperature of isooctane (373 K, see Fig. 6).

This line is inserted in Fig. 6. It should be noted that the temperature is spatially averaged over the film thickness and includes liquid temperature information of the atomizing jet. The fuel temperature in the plenum (290 K) and the boiling temperature of isooctane (373 K) are included in the graph as horizontal dashed lines. The different contact times in the fuel duct lead to different fuel exit temperatures at the orifice region, which are already described in the previous paragraph. The volume flow rate of OP1 is too low to develop a large fuel film with sufficient cooling effect over a wide spatial range. The initial temperature is about 50 K higher compared to OP3. The hot gas crossflow evaporates the fuel film completely within about 10 mm downstream after the orifice center. OP2 and OP3 develop sufficient large cooling films, which extend beyond the field of view. The film temperature of OP2 is initially about 12 K above the temperature of OP3 and it increases faster downstream in comparison to OP3 due to the reduced liquid volume flow and lower evaporation cooling. The maximal average liquid temperature is about 330 K (OP3), about 375 K (OP2) and up to 450 K (OP1). This is above the boiling temperature of isooctane and ethanol, but still below the melting temperature of nile red. Obviously, the liquid is superheated by the locally occurring flame spread due to the fast ignition and combustion. This is also visible in the single-shot images in Fig. 4 for OP1, in which partially spherical flame shapes in the

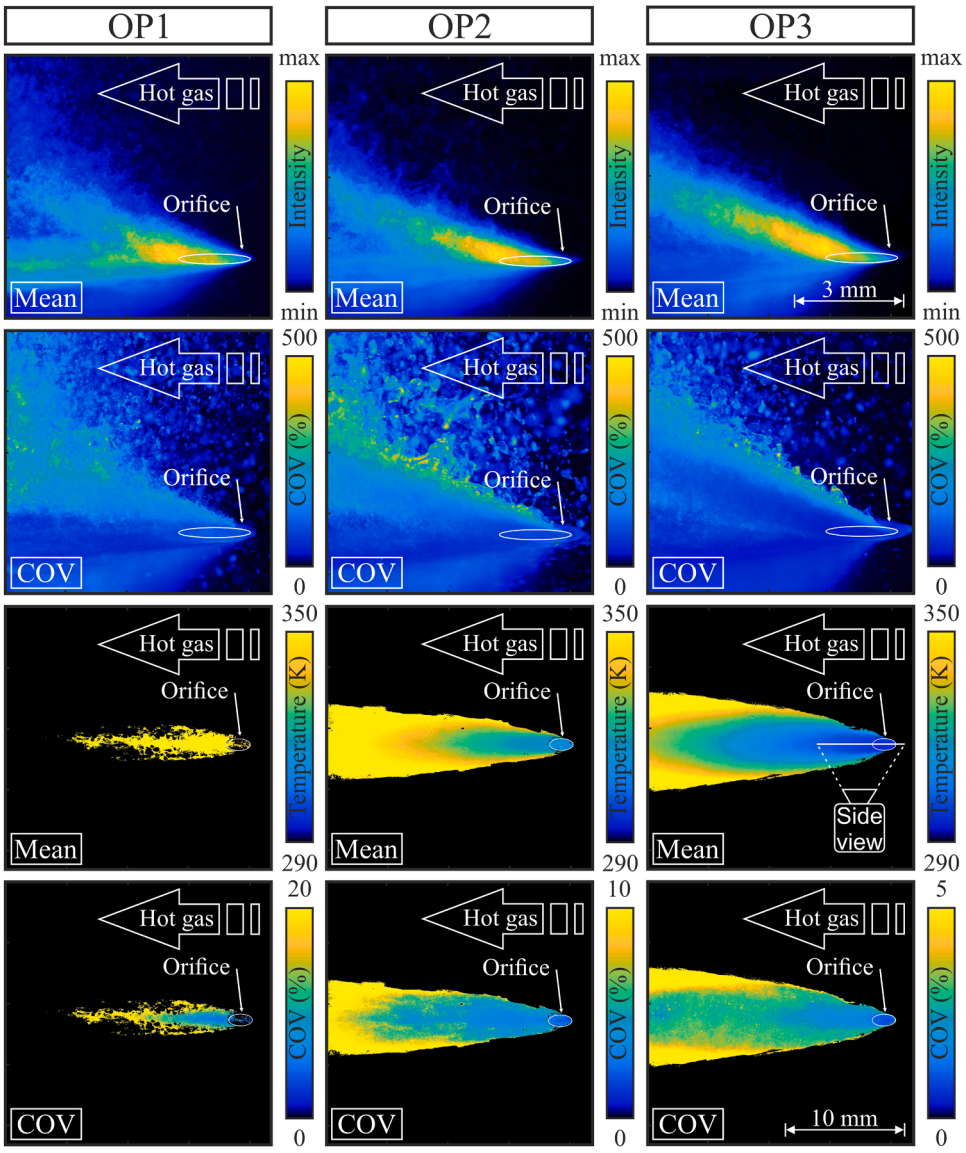


Fig. 5. Mean and COV values for the liquid flow at the orifice (first two lines) and the temperature field (third and fourth lines) for three OPs studied.

cooling liquid (similar like micro-explosions) are visible in the near-nozzle region (about 5 mm downstream). These micro-explosions occur probably due to locally superheated fuel in very hot ambience [20] and are also reported for alcohol/oil flames in the literature [21]. These micro-explosions enhance the liquid jet disintegration and are major cause of secondary droplet breakup in spray flames (e.g. in Flame spray pyrolysis, see [19]. This disintegration mechanism may also accelerate secondary droplets significantly, which can be an explanation for the droplets appearing about 3 mm to 5 mm above the liquid film for OP1 and OP2 (see the single-shot images in Fig. 4). Color photographs of the DSLR camera with and without injection are shown in Fig. 7.

The photos were taken at the same operating conditions but not simultaneously with the LIF measurements. The temperature and pressure detection can be seen on the left side. The wetted surface increases from OP1 to OP3 due to increased flow rate (see Fig. 5, Fig. 7). The wetted surface of OP1 appears longer in comparison to the temperature distribution in Fig. 5. This partial wall wetting does not contribute to a sufficient wall cooling in a large region. The color pictures also show a blue flame luminosity caused by premixed combustion of the fuel film. The blue flame luminosity is reflected on the shiny walls of the measurement section and leads to an illumination also further upstream. The glowing metal tube of the absolute pressure probe and the thermocouple in the color images indicate an increased cooling effect of the bottom near-wall layer of the exhaust flow with increasing fuel volume flow (OP2 and OP3).

3.4. Uncertainty analysis

The applied LIF-technique is ratio-based and thus less dependent on absolute signal intensities. However, ambient signals (e.g. flame luminosity) or a decrease in SNR would lead to increased measurement uncertainties. Appropriate bandpass filters and short integration times reduce the influence of ambient signals on the fluorescence. Consequently, the flame luminosity was not detected with the LIF measurements using the sCMOS cameras in the present paper.

A thermal degradation of the dye in the liquid can be neglected, since the melting point of the dye at 476 K-479 K is not reached in the measurement section [12]. A partial evaporation of the film would lead to an enrichment of the remaining tracer. A larger dye concentration would increase fluorescence re-absorption, so that the fluorescence spectrum may be altered and the film temperature would be over-predicted. However, for thin films this effect is considered to be low but requires further investigation.

Multiple illumination of thin liquid films at high laser fluence would

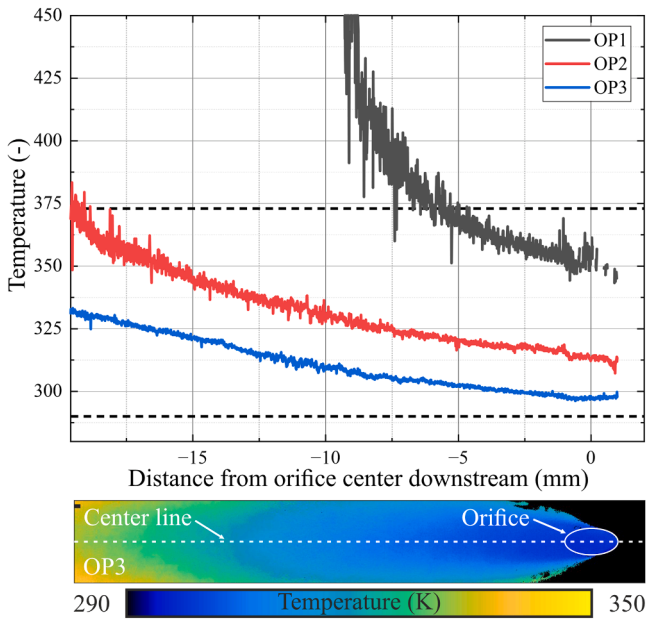


Fig. 6. Temperature plots (along center line) for various operating points (top) and corresponding example average temperature distribution of OP3 (bottom).

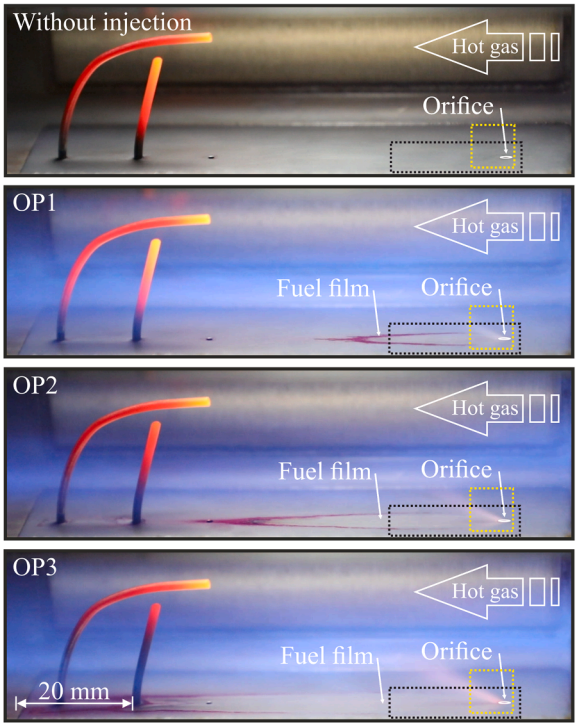


Fig. 7. Color photos before (top) and during fuel injection for various operating points. Dotted rectangles visualize the LIF detection areas of top and side view.

lead to a decrease of the fluorescence intensity of the dye due to photodegradation [10,22]. This would lead to lower SNRs, which consequently would increase the measurement uncertainties. The low residence time of the liquid-tracer mixture in the measurement section and the mixing with fresh fuel/dye due to the high velocity crossflow effectively reduces effects of a multiple illumination at an excitation frequency of 10 Hz. This effect has to be considered, if a measurement at high repetition rate is being pursued.

In the present study a determination of the temperature measurement uncertainty of the single-shot measurements is hardly possible as no other technique is available for comparison. However, the uncertainty of the static 2colour-LIF calibration measurements are available at a film thickness of 0.5 mm (see Fig. 3). The shot-to-shot precision (COV) of the two individual detection channels CH1 and CH2 of the calibration measurements (see Fig. 4) are between 0.052 % (313 K) and 0.263 % (293 K), the spatial COV are between 2.04 % (313 K) to 2.19 % (343 K).

4. Conclusion

In this paper, a liquid film cooling process under rocket-like conditions was analyzed. A hot exhaust gas flow was generated with a pulsejet engine. The fuel mixture for cooling consisting of 90 vol.% isooctane and 10 vol.% ethanol, doped with the fluorescence tracer Nile red was injected under 30° into the hot exhaust gas flow (1070 K, ~ 95 m/s). The highly fluctuating liquid cooling film structure was analyzed with 1-color planar LIF imaging in the orifice region and with a two-color LIF detection scheme to determine the temperature distribution of the liquid flow in a larger ROI also further downstream. The relative temperature sensitivity of the 2c-PLIF in the studied temperature range was always above 1.45 %/K.

The hot wall preheats the exiting fuel in the fuel duct from 290 K to about 294 - 340 K at the nozzle orifice depending on the studied operating point. An increasing flow rate reduces the contact time and consequently the liquid temperature rise in the fuel duct.

The hot exhaust cross flow reacts with the exiting disrupted fuel stream and the formed fuel film leading to locally occurring diffusive combustion events in the orifice region, the edge regions and in the film further downstream. Overall, a premixed flame was observed above the cooling film. The two-color LIF technique enables the determination of a quantitative temperature distribution and an evaluation of the effective cooling length of the fuel films. The effective film length increases with increasing liquid flow rate. The measurements revealed maximal film temperatures in the range of the boiling temperature of isooctane (373 K) at the edge regions and downstream for OP2, while the liquid structures showed superheating for OP1. This may lead to micro-explosions and explains the disintegration of the film in form of locally spherical widening of the liquid film in the near-nozzle region observed for OP1 and partially for OP2.

Measurements without laser illumination revealed, that the flame luminosity is not detected by the two detection channels due to the short integration times of the sCMOS cameras and sufficient bandpass filters.

The signal intensities of CH1 and CH2 at the edge regions and further downstream are very low, indicating small liquid film thickness in these specific regions. Therefore, the low SNRs may lead to locally higher measurement errors of the film temperature in these regions.

The measurements revealed that the temperature distribution of the film and possible non-premixed film or droplet combustion within the field of view is strongly dependent on the structure of the exiting fuel jet and its attachment to the wall. A high flow rate generates a dense, less disrupted fuel stream with reduced liquid surface interacting with the hot exhaust gas, which effectively reduces the occurrence of combustion events at early stages. Otherwise, a disrupted liquid fuel film occurs with formation of ligaments, droplets and larger wrinkling of the liquid surface due to interaction of the turbulent flow of the ambient gas and probably puffing phenomena. Future work will include high repetition rate measurements if the film movement as well as optical measurements of the wall temperature and a further variation of the momentum ratio. This will give deeper insights into the heat transfer under these challenging conditions as well as delivers data for model development required for optimization of the cooling concepts for rocket combustors.

CRediT authorship contribution statement

M. Koegl: conceptualized the experiment, designed the measurement

test rig, manufactured the test rig, performed the measurements, analyzed the data, wrote the paper. B. Andersson: performed the measurements. C. Horsch performed the measurements. M. G. Klatt: performed the measurements, manufactured the test rig. L. Zigan: acquired funding, wrote the paper.

Declaration of competing interest

The authors declare that they have no known competing financial interests or personal relationships that could have appeared to influence the work reported in this paper.

Acknowledgements

We acknowledge financial support by Universität der Bundeswehr München (UniBw M).

References

[1] C.D. Coulbert, Selecting cooling techniques for liquid rockets for spacecraft, J. Spacecr Rocket. 1 (1964) 129–139.
[2] G. Fujii, Y. Daimon, K. Furukawa, C. Inoue, D. Shiraiwa, N. Tanaka, Visualization of coolant liquid film dynamics in hypergolic bipropellant thruster, J. Propuls. Power 38 (2022) 267–273.
[3] S. Soller, H. Riedmann, A. Simonini, J.-B. Gouriet, F. Strauss, C. Kirchberger, C. Dinescu, K. Claramunt, J. Steelant, Experimental and numerical investigation of ethanol film cooling, CEAS Space J. 14 (2022) 187–196.
[4] H. Zhang, J. Zhang, Q. Lin, R. Li, X. Ma, The influence of heat transfer regime and jet parameter on film flow in jet impingement boiling, Int. J. Heat Fluid Flow. 116 (2025) 109948.
[5] S. Tauchi, C. Inoue, Z. Wang, Y. Daimon, G. Fujii, Optimal liquid engine architecture by performance-cooling tradeoff analysis, J. Propuls. Power 40 (2024) 631–641.
[6] K. Murakami, Y. Kamada, Z. Wang, C. Inoue, Hot shear flows promote instabilities of liquid wall films, Int. J. Heat. Mass Transf. 255 (2026) 127783.
[7] B. Hu, Q. Lin, T. Li, W. Li, H. Liu, F. Wang, Flow behavior and heat transfer characteristics of liquid film on vertical hot surface by inclined jet impingement, Int. J. Heat. Mass Transf. 236 (2025) 126387.
[8] C. Liu, Z. Huang, C. Tang, Heat transfer characteristics of oblique jet impingement liquid film cooling in the forced convection mode, Int. J. Heat. Mass Transf. 218 (2024) 124814.
[9] C. Liu, J. Yu, C. Tang, P. Zhang, Z. Huang, The liquid film behaviors created by an inclined jet impinging on a vertical wall, Phys. Fluids 34 (2022).
[10] M. Koegl, L. Breitenbach, Material and surface texture-dependent fluorescence behavior of liquid coolant wall films, Exp. Fluids. 66 (2025) 53.
[11] M. Koegl, C. Mull, K. Baderschneider, J. Wislicenus, S. Will, L. Zigan, Characterization of Nile red as a tracer for laser-induced fluorescence spectroscopy of gasoline and kerosene and their mixture with biofuels, Sensors 19 (2019) 2822.
[12] Carl Roth GmbH & Co. KG (2025) Voluntary safety information following the Safety Data Sheet format according to Regulation (EC) No. 1907/2006 (REACH). Nile red extra pure, Version: 1.0 en. Available online: https://www.carlroth.com/medias/SDB-7726-IE-EN.pdf?context=bWFzdGVyfHNlY3VyaXR5RGF0YXNoZWV0c3wyMjY2ODN8YXBwbGljYXRpb24vcGRmfHNlY3VyaXR5RGF0YXNoZWV0cy9oNWQvaDliLzg5NjUwMTE4MDAwOTQucGRmfGQzYzliZWViOGRlMDU5MGQ0MTMwMDk4YTkwODk5YTgxNGUyZjI2NmJiOTExMzk0Y2FiNzRiZjg0ZWY3OGU1ZGY.
[13] M. Koegl, M. Delwig, L. Zigan, Characterization of fluorescence tracers for thermometry and film thickness measurements in liquid coolants relevant for thermal management of electric and electronic components, Sensors 22 (2022) 8892.
[14] M.R. Vetrano, A. Simonini, J. Steelant, P. Rambaud, Thermal characterization of a flashing jet by planar laser-induced fluorescence, Exp. Fluids. 54 (2013) 1573.
[15] J. Palmer, M.A. Reddemann, V. Kirsch, R. Kneer, Temperature measurements of micro-droplets using pulsed 2-color laser-induced fluorescence with MDR-enhanced energy transfer, Exp. Fluids. 57 (2016) 177.
[16] A.A.H. Pádua, J.M.N.A. Fareleira, J.C.G. Calado, W.A. Wakeham, Density and viscosity measurements of 2,2,4-trimethylpentane (Isooctane) from 198 K to 348 K and up to 100 MPa, J. Chem. Eng. Data 41 (1996) 1488–1494.
[17] ThermoData Engine (TDE103b V10.1) User`s Guide. https://trc.nist.gov/TDE/Help/TDE103b/Eqns-Pure-SurfaceTension/HVPExpansion-SurfaceTension.htm.
[18] M. Huo, S. Lin, H. Liu, C.-F.F. Lee, Study on the spray and combustion characteristics of water–emulsified diesel, Fuel 123 (2014) 218–229.
[19] N. Jüngst, G.J. Smallwood, S.A. Kaiser, Visualization and image analysis of droplet puffing and micro-explosion in spray-flame synthesis of iron oxide nanoparticles, Exp. Fluids. 63 (2022) 60.
[20] R.S. Volkov, P.A. Strizhak, Using planar laser induced Fluorescence to explore the mechanism of the explosive disintegration of water emulsion droplets exposed to intense heating, Int. J. Therm. Sci. 127 (2018) 126–141.
[21] X. Chen, W. Long, Y. Wang, G. Xiao, P. Dong, Z. Wang, X. Xi, Experimental investigation on enhanced combustion of methanol/heavy fuel oil by droplet puffing at elevated temperatures, Sci. Rep. 14 (2024) 14525.
[22] M. Koegl, N. Mil'to, L. Zigan, Simultaneous film temperature and film thickness measurements for jet impingement applications using two-color laser-induced fluorescence, Exp. Fluids 65 (2024) 41.